Evaluation of the effect of engine, load and turbocharger parameters on transient emissions of a diesel engine

C.D. Rakopoulos*, A.M. Dimaratos, E.G. Giakoumis, D.C. Rakopoulos

Internal Combustion Engines Laboratory, Thermal Engineering Department,
School of Mechanical Engineering, National Technical University of Athens,
9 Heroon Polytechniou St., Zografou Campus, 15780, Athens, Greece

Abstract

The vital issue of exhaust emissions during transient operation of diesel engines has been studied so far mainly on an experimental rather than simulation basis, owing to the very high computational times required for the analysis of each transient cycle. The study of transient emissions, however, is extremely important to manufacturers, since newly produced engines must meet the stringent regulations concerning exhaust emissions levels. In the present work, a comprehensive two-zone transient diesel combustion model is used for a preliminary evaluation of the effect of various parameters on nitric oxide (NO) and soot emissions during transient operation after load changes. The parameters are divided into three categories according to the specific sub-system examined, i.e. engine, load and turbocharger. Demonstrative diagrams are provided for the development of NO and soot emissions during the transient event, which depict the effect of each parameter considered. Moreover, the peculiarities of each case are discussed mainly in relation to turbocharger lag effects. For the current engine-load configuration, it is found that exhaust valve opening timing and cylinder wall insulation affect considerably NO and soot emissions. Additionally, load characteristics as well as turbocharger (T/C) mass moment of inertia play an important role on the development of transient NO and soot emissions.

Keywords: Turbocharged diesel engine, Transient operation, NO concentration, Soot density, Parametric study

* Corresponding author. Tel.: +30 210 7723529, Fax: +30 210 7723531.
E-mail address: cdrakops@central.ntua.gr (C.D. Rakopoulos)

Nomenclature

A	surface area (m^2)
D	cylinder bore (m)
E	internal energy (J) or activation energy (J/kmol)
E_{red}	reduced activation energy (K)
G	mass moment of inertia ($kg\,m^2$)
h	specific enthalpy (J/kg)
k_f	forward reaction rate constant (m^3/kmol/s)
L_{rod}	connecting rod length (m)
m	mass (kg)
M	molecular weight (kg/kmol)
N	engine rotational speed (rpm)
p	pressure (N/m^2)
P	combustion model preparation rate (kg/°CA)
Q	heat (J)
r	crank radius (m)
R	combustion model reaction rate (kg/°CA)
R_{mol}	universal gas constant (8314.3 J/kmol/K)
R_i	one-way equilibrium rate for reaction i
S	piston stroke (m)
t	time (sec)
T	temperature (K)
$\bar{u}_{pist}$	mean piston velocity (m/s)
V	volume (m^3)

Greek

θ	temperature (°C)
ρ	density (kg/m^3)
τ	torque (Nm)
φ	crank angle (deg)
Φ	fuel-air equivalence ratio
ω	angular speed (rad/s)

Subscripts

a	air
ch	charge
e	engine or equilibrium
f	fuel
fl	flywheel
fr	friction
g	gas
inj	injected
L	loss or load
sc	soot consumed (oxidized)
sf	soot formed
sn	soot net
up	unprepared
w	wall

Abbreviations

°CA	degree(s) crank angle
EVO	exhaust valve opening
FMEP	friction mean effective pressure (bar)
LHR	low heat rejection
NO	nitric oxide
PSZ	plasma spray zirconia
rpm	revolutions per minute
rps	revolutions per second
SN	silicon nitride
T/C	turbocharger
TDC	top dead center
VGT	variable geometry turbocharger

1. Introduction

The turbocharged diesel engine is nowadays the most preferred prime mover in medium and medium-large units applications (truck driving, land traction, ship propulsion, electrical generation). Moreover, it continuously increases its share in the highly competitive automotive market owing to its reliability that is combined with excellent fuel efficiency. Particularly, its transient operation is of great importance in the everyday operating conditions of engines, being often linked with off-design and consequently non-optimum performance.

As it has long been established, turbocharger lag is the most notable off-design feature of diesel engine transient operation that significantly differentiates the torque pattern from the respective steady-steady conditions. It is caused because, although the fuel pump responds rapidly to the increased fueling demand after a load or speed increase, the turbocharger (T/C) compressor air-supply cannot match this higher fuel-flow instantly, but only after a number of engine cycles owing to the inertia of the whole system (since there is no mechanical connection between engine crankshaft and turbocharger); the above phenomenon is enhanced by the unfavorable T/C compressor characteristics at low loads and speeds. As a result of this slow reaction, the relative air-fuel ratio during the early cycles of a transient event assumes very low values (even lower than stoichiometric), thus deteriorating combustion and leading to slow engine (torque and speed) response, long recovery period and overshoot in particulate, gaseous and noise emissions. On the other hand, the high fuel-air equivalence ratios experienced after a speed or load increase transient event produce high combustion temperatures, which favor nitric oxide (NO) and soot formation, with the latter being identified as black smoke coming out of the exhaust pipe [1].

During the last decades, the modeling of the thermodynamic and gas dynamic processes and combustion in diesel engines has intensively supported the study of engine operation under transient conditions, with simulations of various levels of complexity. Extensive studies have been conducted for a variety of purposes, such as investigation of the effect of various parameters on engine transient response and performance [1-4], ways of improving response [1,5], compressor surging [6], second-law balance [7] and issues concerning engine dynamics [8].

On the other hand, the vital issue of exhaust emissions under transient operating conditions of diesel engines - although of primary concern to engine manufacturers since newly produced engines must meet the stringent emissions regulations following

a legislated Transient Cycle - has been investigated so far mainly on an experimental rather than simulation basis [9,10]. Incorporation of exhaust emissions prediction into transient simulations would lead to high or even prohibitive computational times. Thus, most of the transient models do not include prediction of exhaust emissions via the use of a multi- or even a two-zone combustion model, with only very few exceptions [11-14], with references [13] and [14] addressing only prediction of NO emission. On the other hand, approximations using quasi-linear models, which are based on steady-state engine philosophy, fail to predict accurately transient emissions, especially so for the turbocharger lag cycles [10], since no actual modeling of the relevant off-design phenomena that occur under transient conditions is included.

The aim of this paper is a preliminary evaluation of the effect of various engine, load and turbocharger parameters on transient NO and soot emissions of a heavy-duty diesel engine. For this purpose, a comprehensive two-zone diesel combustion model is integrated into an experimentally validated transient simulation code, having the added advantage of limited requirements in terms of computer memory and execution time. Detailed modeling of all in-cylinder processes (i.e. air motion, fuel spray development, wall impingement and combustion chemistry) is included, while analytical equations provide an in depth description of the phenomena that differentiate transient from steady-state operation. The parameters considered in the study are divided into three categories: i) engine parameters, including exhaust manifold volume, exhaust valve opening (EVO) timing, cylinder wall insulation (low heat rejection-LHR engine) and lubricating oil, ii) load parameters comprising of type, final magnitude and change duration, and iii) turbocharger (T/C) parameters, including mass moment of inertia and geometric turbine inlet area (as a feature of variable geometry turbocharger-VGT configuration).

The results of the analysis are given in a series of demonstrative diagrams, which depict the effect of each parameter considered on NO and soot exhaust emissions of a diesel engine, during transient operation initiated by a load increase. Additionally, the development of important variables, which strongly influence NO and soot emissions evolution during the transient event (e.g. fuel-air equivalence ratio), or closely related to the examined parameter (e.g. turbocharger response when the effect of T/C mass moment of inertia is studied) are given in each diagram.

The paper is organized as follows: Firstly, a brief description of the two-zone thermodynamic model is given, followed by the analysis of combustion products

calculation. Afterwards, the basic points of the engine dynamic model are given and, then, the results of the study are presented and discussed in detail, mainly in relation to turbocharger lag effects. Finally, the basic features of the study are summarized briefly and the main conclusions are highlighted.

2. Thermodynamic modeling

2.1 Two-zone model description – conservation and state equations

The thermodynamic model incorporates all the processes taking place in the cylinder, i.e. in-cylinder air motion, fuel spray development and mixing, spray impingement on the walls, turbulent heat transfer and combustion chemistry. Droplets evaporation and fuel ignition delay are implicitly taken into account through the combustion sub-model. The fuel is assumed to be dodecane ($C_{12}H_{26}$) with a lower heating value LHV=42,500 kJ/kg. The evaluation of the thermodynamic processes is based on the first law of thermodynamics and the perfect gas state equation. Detailed description of the model can be found in [15,16]. In this paper, a brief description of the model's main features will be given.

Two separate zones in the cylinder are identified, namely the air (unburned) zone consisting of pure air, and the fuel spray (burned) zone consisting of the combustion products, injected fuel and the incoming air from the air-zone. During compression only one zone exists (that of pure air). Thus, the first law of thermodynamics for a closed system and the perfect gas state equation read [17]:

$$dQ = dE + pdV \tag{1}$$

$$pV = m\frac{R_{mol}}{M_{ch}}T \tag{2}$$

where dQ is the heat loss to the cylinder walls, M_{ch} the charge molecular weight and V the instantaneous cylinder volume given as function of crank angle φ by

$$V(\varphi) = V_{cl} + \frac{\pi D^2}{4}\left[r(1-\cos\varphi) + L_{rod}(1-\sqrt{1-\lambda^2\sin^2\varphi})\right] \tag{3}$$

where V_{cl} is the cylinder clearance volume and $\lambda=r/L_{rod}$ the crank radius to connecting rod length ratio.

During combustion and expansion, both unburned and burned zones exist; the latter consists of all fuel sprays developed in the cylinder according to the number of injector

nozzle holes. In this case, apart from the perfect gas state equation, the first law of thermodynamics for an open system is applied for each zone.

For the surrounding air-zone, which only loses air mass to the burning zone, the first law of thermodynamics is expressed by [18]:

$$dQ = dE + pdV + h_a dm_a \tag{4}$$

while for the burning zone, which gains air mass from the air-zone and also an enthalpic flow from the fuel prepared to be burned in the time step, the first law of thermodynamics is written in the form:

$$dQ = dE + pdV - h_a dm_a - h_f dm_f \tag{5}$$

Polynomial expressions according to the absolute temperature T are used concerning the calculation of internal energy and specific heat capacities for each species considered in the model [18]. Internal energy E in the above equations is then computed by knowing the instantaneous composition (by the combustion chemistry sub-models) and the specific internal energy of each constituent. Internal energy terms include sensible and heat of formation parts.

After the calculation of the state in each zone, a mean state of the cylinder contents can be computed assuming isenthalpic mixing of the zones [15].

2.2 Heat transfer model

The improved model of Annand and Ma [19] is used for the calculation of the heat transfer rate between in-cylinder gas and surrounding cylinder walls:

$$\frac{dQ_L}{dt} = A\left\{\frac{k_g}{D}Re^b\left[a(T_g - T_w) + \frac{a'}{\omega}\frac{dT_g}{dt}\right] + c(T_g^4 - T_w^4)\right\} \tag{6}$$

where a, $a^{/}$, b and c are constants evaluated after experimental matching at steady-state conditions. Further, $A=2A_{pist}+ A'$, with $A_{pist}=\pi D^2/4$ the piston cross section area and $A'=\pi Dx$, with x the instantaneous cylinder height in contact with the gas (including the height of clearance volume). Also, T_g is the absolute zone temperature and $Re = \rho \bar{u}_{pist} D / \mu_g$ is the Reynolds number; $\bar{u}_{pist} = 2NS/60$ is the mean piston speed with S the piston stroke, and k_g, μ_g are the gas thermal conductivity and viscosity, respectively, expressed as polynomial functions of temperature T_g [18,20]. After the start of combustion (when both unburned and burned zones exist), total heat loss to the cylinder walls is distributed into the two zones in proportion to their mass and absolute temperature [18,21].

During transient operation, the thermal inertia of the cylinder wall is taken into account, using a detailed heat transfer scheme that models the temperature distribution from the gas to the cylinder walls up to the coolant (convection and radiation from gas to internal wall surface, conduction across the cylinder wall and convection from external wall surface to coolant) [22].

2.3 Combustion model

The calculation of the combustion rate is based on the model proposed by Whitehouse and Way [23]. In this model, the combustion process consists of two parts; a preparation limited combustion rate and a reaction (Arrhenius type) limited combustion rate.

The preparation rate P (in kg/°CA) is given by:

$$P = K m_{f_{inj}}^{1-x} m_{f_{up}}^{x} p_{O_2}^{m} \tag{7}$$

while the reaction rate R (in kg/°CA) is defined as:

$$R = \frac{K' p_{O_2}}{N' \sqrt{T}} e^{-E_{red}/T} \int_0^{\varphi} (P - R)\, d\varphi \tag{8}$$

In the above relations, $m_{f_{inj}}$ is the cumulative fuel mass injected up to the current crank angle φ, which is expressed as:

$$m_{f_{inj}} = \int_0^{\varphi} \frac{dm_{f_{inj}}}{d\varphi} d\varphi \tag{9}$$

where $dm_{f_{inj}} / d\varphi$ is the fuel injection rate. Moreover, $m_{f_{up}}$ is the cumulative fuel mass not yet prepared for combustion and is calculated by the relation:

$$m_{f_{up}} = m_{f_{inj}} - \int_0^{\varphi} P d\varphi \tag{10}$$

Also, N' is the engine speed in revolutions per second (rps) and p_{O_2} is the oxygen partial pressure (in bar) in the burning zone. Constants K, K', x, m and E_{red} are evaluated after experimental matching at steady-state conditions.

Finally, the combustion rate is defined by the following relations:

$$\frac{dm_{fb}}{d\varphi} = \begin{cases} R, & \text{if } R<P \\ P, & \text{if } R>P \end{cases} \tag{11}$$

3. Calculation of combustion products

3.1 Chemistry of combustion - Chemical equilibrium

The complete chemical equilibrium scheme proposed by Way [24] is adopted for the calculation of combustion products, which are defined by dissociation considerations. The species considered are N_2, O_2, CO_2, H_2O, CO, H_2, NO, OH, N, H and O. The concentration of each one of the above species is calculated by solving a system of eleven equations, consisting of four atom balances (one for each element of the system C-H-O-N) and seven equilibrium equations. The chemical reactions considered in equilibrium, together with their respective equilibrium constants, are the following:

$$
\begin{aligned}
&(1)\ \ N_2 + O_2 \rightleftharpoons 2NO, && K_{p1} = p_{NO}^2 \Big/ \left(p_{N_2} \cdot p_{O_2}\right) \\
&(2)\ \ 2H_2O + O_2 \rightleftharpoons 4OH, && K_{p2} = p_{OH}^4 \Big/ \left(p_{H_2O}^2 \cdot p_{O_2}\right) \\
&(3)\ \ 2CO + O_2 \rightleftharpoons 2CO_2, && K_{p3} = p_{CO_2}^2 \Big/ \left(p_{CO}^2 \cdot p_{O_2}\right) \\
&(4)\ \ 2H_2 + O_2 \rightleftharpoons 2H_2O, && K_{p4} = p_{H_2O}^2 \Big/ \left(p_{H_2}^2 \cdot p_{O_2}\right) \\
&(5)\ \ N_2 \rightleftharpoons 2N, && K_{p5} = p_N^2 / p_{N_2} \\
&(6)\ \ H_2 \rightleftharpoons 2H, && K_{p6} = p_H^2 / p_{H_2} \\
&(7)\ \ O_2 \rightleftharpoons 2O, && K_{p7} = p_O^2 / p_{O_2}
\end{aligned}
\qquad (12)
$$

where p_i are the partial pressures of the species, made dimensionless with respect to atmospheric pressure p_{atm} = 1 atm.

3.2 Nitric oxide formation

As it is well established that NO formation cannot be predicted accurately by chemical equilibrium considerations, the generally accepted chemical kinetics model proposed by Lavoie et al. [25] is used; it describes the extended Zeldovich kinetics scheme. According to this model, the governing chemical reactions for NO formation and their respective forward reaction rate constants are as follows:

$$
\begin{aligned}
&N + NO \rightleftharpoons N_2 + O, && k_{1f} = 3.1\times10^{10} e^{(-160/T)} \\
&N + O_2 \rightleftharpoons NO + O, && k_{2f} = 6.4\times10^{6} T e^{(-3125/T)} \\
&N + OH \rightleftharpoons NO + H, && k_{3f} = 4.2\times10^{10}
\end{aligned}
\qquad (13)
$$

The respective one way equilibrium rates for the above reactions are defined as:

$$
R_1 = k_{1f}(N)_e(NO)_e, \quad R_2 = k_{2f}(N)_e(O_2)_e, \quad R_3 = k_{3f}(N)_e(OH)_e \qquad (14)
$$

where index ‘e’ denotes equilibrium concentrations and term $\alpha = (NO)/(NO)_e$.

Finally, the rate of change of NO concentration is expressed as follows:

$$\frac{1}{V}\frac{d\left((NO)V\right)}{dt} = 2\left(1-\alpha^2\right)\frac{R_1}{1+\alpha\dfrac{R_1}{R_2+R_3}} \tag{15}$$

3.3 Net soot formation

The model proposed by Hiroyasu et al. [26], as modified by Lipkea and DeJoode [27], is adopted for the calculation of the net soot formation rate. The latter is defined as the difference between the formation and oxidation rates, which are given, respectively, by:

$$\frac{dm_{sf}}{dt} = A_{sf} dm_f^{0.8} p^{0.5} e^{\left(-E_{sf}/(R_{mol}T)\right)} \tag{16}$$

$$\frac{dm_{sc}}{dt} = A_{sc} m_{sn} \left(p_{O_2}/p\right) p^n e^{\left(-E_{sc}/(R_{mol}T)\right)} \tag{17}$$

where pressures are in bar and masses in kg, dm_f is the fuel vapor mass to be burned in the current time (crank angle) step, and p_{O_2} is the partial pressure of oxygen in the zone. Also, constants A_{sf}, A_{sc}, activation energies E_{sf}, E_{sc} and the exponent n are evaluated after experimental matching at steady-state conditions. Finally, the net soot formation rate is expressed as follows:

$$\frac{dm_{sn}}{dt} = \frac{dm_{sf}}{dt} - \frac{dm_{sc}}{dt} \tag{18}$$

4. Dynamic Analysis

4.1 Crankshaft torque balance

The conservation of angular momentum applied to the total system (engine plus load), based on Newton's second law of motion, is given by:

$$\tau_e(\varphi,\omega) - \tau_{fr}(\varphi,\omega) - \tau_L(\omega) = G_{tot}\frac{d\omega}{dt} \tag{19}$$

where G_{tot} is the total mass moment of inertia of the system (engine-flywheel-brake) reduced to the crankshaft axis. The term $\tau_e(\varphi,\omega)$ represents the instantaneous engine indicated torque and includes gas, inertia and (the negligible) gravitational forces contribution; it is mostly dependent on accurate combustion modeling [8].

For the calculation of friction torque $\tau_{fr}(\omega)$ inside the cylinder, a detailed model is applied [8]. According to this approach, the total amount of friction at each degree crank

angle (°CA) is the summation of four terms, i.e. piston rings assembly (including piston rings and piston skirt contribution), loaded bearings, valve train and auxiliaries. The advantage, here, is that the considerable variation of friction torque during the engine cycle is taken into account, unlike the usually applied 'mean' fmep equations where friction torque is assumed constant throughout each cycle.

Finally, $\tau_L(\omega)$ is the load torque, given by:

$$\tau_L(\omega) = C_1 + C_2\omega^s \tag{20}$$

For a linear load-type (i.e. electric brake, generator) s=1, for a quadratic load-type (i.e. hydraulic brake, vehicle aerodynamic resistance) s=2, with C_1 the speed-independent load term (e.g. road slope).

4.2 Multi-cylinder engine modeling

At steady-state operation the performance of each cylinder of a multi-cylinder engine is practically the same, due to the practically fixed position of the mechanical fuel pump rack position, resulting in the same amount of fuel being injected per cycle, and the fixed turbocharger compressor operating point resulting in the same air mass flow-rate for each cylinder. On the other hand, under transient conditions each cylinder experiences different fueling and air mass flow-rate during the same engine cycle. This is the result of the combined effect of a) the continuous movement of the fuel pump rack, initiated by a load or speed change, and b) the continuous movement of the turbocharger compressor operating point. As regards speed changes, only the first cycles are practically affected, but, when load changes are investigated (as is the case with the present study), significant variations can be experienced throughout the whole transient event.

The usual approach, here, is the solution of the governing equations for one cylinder and the subsequent use of suitable phasing images of this cylinder's behaviour for the others. This approach is widely applied due to its low computational time. Unlike this, a true multi-cylinder engine model is incorporated into the simulation code [1]. In this model, all the governing differential and algebraic equations are solved separately for each cylinder, according to the current values of fuel pump rack position and turbocharger compressor air mass flow-rate. This causes significant differences in the behaviour of each cylinder during the same transient cycle, affecting, among other things, engine response and exhaust emissions.

4.3 Fuel pump operation

Instead of applying the steady-state fuel pump curves during transients, a fuel injection model, experimentally validated at steady-state conditions, is used. Thus, simulation of the fuel pump-injector lift mechanism is accomplished, taking into account the delivery valve and injector needle motion. The unsteady gas flow equations are solved (for compressible injected fuel flow) using the method of characteristics, providing the dynamic injection timing as well as the duration and the rate of injection for each cylinder at each transient cycle. The obvious advantage here is that the transient operation of the fuel pump is also taken into account. This is mainly accomplished through the fuel pump residual pressure value, which is built up together with the other variables during the transient event.

5. Experimental procedure

The experimental investigation was carried out on a six-cylinder, four-stroke, moderately turbocharged and aftercooled diesel engine of 16.6 lt total displacement volume and tight governing; the cylinder bore is 140 mm, the piston stroke is 180 mm, and the rated power 236 kW at 1500 rpm.

The first task was the investigation of the steady-state performance of the engine in hand. For this purpose, an extended series of steady-state trials was conducted in order on the one hand to examine the model's predictive capabilities and, on the other, to calibrate successfully the individual sub-models described in the previous sections. The calculated values of the constants of each sub-model, which are within the well established corresponding ranges [18,27], remained then constant for all the other examined cases.

The next task was the investigation of the transient operation. Owing to the narrow speed range (1000-1500 rpm) of the particular engine, mainly load changes (increases) with constant governor setting were examined. An important feature of the engine under study is its very high mass moment of inertia (3 to 4 times greater than in similar configurations), which tends to limit the transient effects of the variables examined. Typical results of the experimental investigation are given in Figure 1 for a 10-50% load increase commencing from 1180 rpm. The non-linear character of the load application, which could not be accounted for in the simulation, is responsible for the small differences observed in boost pressure and engine speed response. The particular

hydraulic brake has a very high mass moment of inertia, resulting in long, abrupt and non-linear actual load change profiles. Nonetheless, the matching between experimental and predicted transient responses seems satisfactory for all measured engine and turbocharger variables (engine speed, fuel pump rack position and boost pressure); it is, thus, believed to form a sound basis for the theoretical study of transient exhaust emissions that follows.

6. Results and discussion

6.1 Nominal transient event

Figure 2 illustrates the engine and turbocharger response during a 10-80% increase in engine load at constant governor setting, which forms the nominal case for the parametric study that follows. As expected, engine speed drops after the application of the new higher load owing to the torque deficit between engine and resistance (load). This is sensed by the governor, which responds by moving the fuel pump rack to an increased fueling position. At the same time, the turbocharger as well as the other system lags cause a delay in boost pressure build-up and, thus, shortage of combustion air is experienced resulting in a rapid decrease of the air-fuel equivalence ratio (recall that aerodynamic type compressors cannot achieve high air mass flow-rates at low turbocharger speeds). However, the very high mass moment of inertia of the current engine slows down the whole transient event development and prevents complete combustion deterioration during the early cycles.

Figure 3 focuses on the development of NO exhaust emission for the nominal load increase transient event of Figure 2; the maximum value of the mean (comprising both burned and unburned zones contribution) temperature in each transient cycle as well as the oxygen concentration in the fuel spray are also provided for comparison purposes. Initially, NO emissions are quite low owing to the low values of the fuel-air equivalence ratio and charge temperature at the initial low loading. As the load increases, NO emissions increase too with its development following closely the temperature profile. This was intuitively expected based on the, well known, strong dependence of NO formation on temperature (already documented in Equation (13)). In the case of NO emissions, it is, primarily, the lag between increased fueling and the response of the air-charging system that is responsible for the increased emissions noticed in Figure 3 (in engines equipped with exhaust gas recirculation, the EGR starvation during the first cycles of a load increase or acceleration transient event enhances the above trend). On

the other hand, the injection pressure and exhaust pressure history play a secondary but non-negligible role [10]. Since the main parameter affecting NO formation is the burned gas temperature, local high temperatures due to close to stoichiometric air-fuel mixtures increase NO emissions during the turbocharger lag cycles as it is obvious in Figure 3 up to the 25^{th} cycle. At the same time, the cylinder wall temperature is still low, as the 'thermal' transient develops much slower owing to the thermal inertia of the cylinder wall-coolant system; this functions in an opposite manner, as it actually leads to higher heat transfer rates to the cylinder walls according to Equation (6), hence slight reduction of the gas temperature. The latter, however, only moderately limits the general strong and monotonic increasing trend of NO with Φ.

Another primary mechanism that affects NO formation is the in-cylinder oxygen availability. The latter parameter is illustrated in Figure 3 in terms of oxygen concentration in the fuel spray, where the conditions are mostly favorable for NO formation. Following the rapid decrease in the air-fuel ratio, oxygen concentration is rather limited during the turbocharger lag cycles. However, owing to the peculiarities of the particular engine (i.e. high mass moment of inertia that slows down the transient event) the relative air-fuel ratio never dropped below the stoichiometric value (see also Figure 2), which means that oxygen was always available for NO formation in the fuel spray.

Figure 4 expands the previous analysis by illustrating soot exhaust emission as well as the maximum value of the mean (comprising both burned and unburned zones contribution) temperature in each transient cycle and fuel-air equivalence ratio developments for the same load increase transient event. It is a well known fact that the formation of soot is mainly dependent on engine load [17]. As the load increases, more fuel is injected into the cylinders, increasing the temperatures in the fuel-rich zone during diffusion combustion; thus, the formation of soot is favored. The local high values of fuel-air ratio experienced during turbocharger lag enhance the above mechanism, which is more pronounced the higher the engine rating. At the same time, soot oxidation proceeds more slowly owing to the lower partial pressure of oxygen in the fuel spray (caused by poorer mixing). For the overshoot in soot emissions observed in the first seconds of the transient event of Figure 4, therefore, the main cause is the instantaneous lack of air due to turbocharger lag, aided by the initial sharp increase in ignition delay during the early transient cycles.

Recent investigation by the present research group has also identified the following very interesting findings:

- Transient exhaust emissions develop in a different way compared to the respective steady-state ones, owing to the differentiated fuelling and air-mass flow-rates experienced during transients. Both NO and soot emissions assume higher exhaust values during transients than in the respective steady-state conditions.
- NO formation is retarded for a few degrees CA during the transient cycles compared to steady-state conditions, owing to the overall slowing down of the whole combustion process during turbocharger lag.
- Soot formation and oxidation proceed more slowly during a transient cycle compared to its steady-state counterpart, resulting in lower in-cylinder maximum but higher exhaust values of soot density since the soot oxidation rate is actually lower than the formation one.

In the previous paragraphs, the main mechanisms of NO and soot formation during a typical transient event were described. These form the basis for the parametric analysis that follows.

6.2 Effect of engine parameters

Figure 5 addresses the effect of exhaust manifold volume on NO and soot emissions during transient operation after a load increase. The development of the exhaust manifold pressure is also presented for comparison purposes. In the case of a very large exhaust manifold (resembling a constant pressure turbocharging system), the intake system flow inertia increases considerably slowing down the exhaust manifold pressure build up and resulting in much lower turbocharger speed and, thus, lower boost pressure produced by the T/C compressor compared to the nominal operation. Then, the combined effect of low air-supply and increased fueling (recall that the governor has responded to the speed drop by forcing the fuel pump rack to increase fueling) produces high values of fuel-air equivalence ratio, increasing accordingly both NO and soot emissions. On the other hand, a very small exhaust manifold improves only moderately the engine response and the exhaust emissions, mainly, owing to the slightly increased levels of exhaust manifold and boost pressures.

The latter finding confirms the results of Watson [5] who argued that further decrease of the exhaust manifold volume from the optimum brings no beneficial effects.

Figure 6 presents the effect of exhaust valve opening (EVO) timing on transient NO and soot emissions. In this figure, the fuel-air equivalence ratio and boost pressure developments are also given for comparison purposes. Valve timing plays an important role from the engine configuration point of view, as it determines the pressure and temperature of the exhaust gas leaving the cylinder. The higher this level the higher the available energy at the turbine inlet, reducing accordingly the turbocharger lag and aiding faster engine speed response and lower smoke emissions. Historically, early opening of the exhaust valve was proposed as a viable means for improving transient performance [1], however at the expense of lower engine efficiency since only part of the potential expansion work is actually obtained. By advancing the opening of the exhaust valve, the effective expansion stroke is reduced and the balance of fuel energy conversion is altered with a significant part transferred from the piston to the turbine.

Two modifications of the nominal EVO timing are examined in Figure 6, i.e. 30 °CA advanced and 20 °CA retarded. As shown in Figure 6, NO emission is increased either by advancing or retarding EVO timing, while soot emission increases only in the case of advanced EVO timing. Different mechanisms lie behind these trends. On the one hand, soot density in the exhaust obtains significantly higher values (up to 50% in the current study) with advanced EVO timing, due to the lesser available time for its oxidation during expansion as well as due to the smaller cylinder volume at the EVO event. This can be also documented in the sub-diagram inside Figure 6, which shows the development of NO concentration and soot density during the closed part of the engine cycle. In the reverse case (retarded EVO timing), soot density in the exhaust assumes lower values.

On the other hand, NO emission is mainly influenced by the maximum cycle temperature, which is directly affected by the fuel-air equivalence ratio. An earlier opening of the exhaust valve causes a reduction in piston work, since it shortens the effective expansion stroke, leading ultimately to greater speed droops. This forces the governor to increase fueling even more. At the same time, the energy delivered to the turbine is higher, leading to higher boost pressures. The combination of increased fueling and boost pressure ultimately leads to higher values of fuel-air equivalence ratio, as shown in Figure 6, and thus higher peak temperatures and NO emission. In the

case of retarded EVO, the opposite behavior is observed, but the combination of boost pressure and fueling produces again high fuel-air equivalence ratios leading to increased levels of NO emission.

The very interesting case of insulated cylinder walls, resembling a low heat rejection (LHR) engine, is investigated in Figure 7. Two common insulators are examined, i.e. plasma spray zirconia (PSZ; 1.0 and 1.5 mm thickness coating) and silicon nitride (4.0 mm thickness coating). The objective of a LHR engine is to minimize heat loss to the cylinder walls, eliminating in that way the need for a cooling system. This is achieved at the expense of increased levels of gas temperatures inside the cylinder, resulting from the insulation applied to the cylinder walls, piston crown, cylinder head and/or valves. Also, the gas-side wall temperatures are significantly increased, as illustrated in Figure 8. At the same time, its effect on engine and turbocharger transient response has been reported to be very limited [22]. As a result, the highly insulated cylinder wall cases exhibit higher NO emissions, owing to its strong dependence on gas temperature as dictated by equation (13). On the other hand, soot emissions seem to be affected only moderately, showing a slight increase for higher degrees of insulation. This is attributed to the combined effect the higher gas temperature has on both the soot formation and oxidation processes, as shown in equations (16) and (17).

Figure 8 depicts the lubricating oil (type and temperature) effect on transient NO and soot emissions after a load increase. Also, the engine speed response and the friction mean effective pressure development, as calculated by a detailed sub-model [8], are provided. Two different oils are examined, i.e. SAE 30 and SAE 20W50, at different temperatures which correspond to fully warmed-up and cold-starting conditions. The basic property of the lubricating oil is its viscosity, which is dependent upon its type and temperature, and directly affects friction losses; it is calculated by the Vogel equation [8]. Low viscosity reduces friction, thus increased oil temperature is generally desirable. In the case of lower oil temperature (for the same oil type), friction torque is significantly increased throughout the whole engine cycle, leading to greater speed droops, as dictated by equation (19). This in turn causes higher fueling rates in order to respond to the load increase, resulting in higher values of fuel-air equivalence ratio. The latter leads to increased levels of NO and soot emissions. In order to further support this, an even more extreme oil type/temperature case is examined, namely SAE20W50 oil at 40 °C. Here, the oil viscosity is even higher, producing higher friction torque and

causing even greater speed droops and fueling rates, ultimately leading to elevated NO and soot emissions levels.

6.3 Effect of load parameters

Figure 9 highlights the effect of the magnitude of the applied load on NO and soot exhaust emissions during transient operation. Obviously, the higher the applied load, the higher the (engine minus load) torque deficit during the early cycles of the transient event. This, in turn, leads to greater engine speed droops, forcing the governor to move the fuel pump rack to higher fueling position. The latter, combined with the 'harder' turbocharger lag period (since air mass flow rate from the T/C compressor must now meet the much increased fueling rate) for the higher applied loads, leads to greater values of fuel-air equivalence ratio and, thus, higher cylinder peak pressures and temperatures. These conditions are favorable for NO and soot formation, with turbocharger lag effects being more pronounced the higher the applied load. The latter phenomenon leads to higher peaks of both emissions. Additionally, cumulative mass values of NO and soot emissions are also increased for higher loads, as documented in Figure 9. In the case of the 10-90% load increase, the cumulative mass values are much greater due to the fact that more cycles were needed for the engine to reach the final equilibrium after the new load was imposed.

Figure 10 presents the development of NO and soot emissions during transient operation after a load increase for various, realistic load-time schedules. As it can be seen, this parameter affects significantly the development profile and peak values of both emissions. On the other hand, consistent with engineering intuition, the final equilibrium conditions are practically the same for all the cases examined. The worst case for both emissions is the instant load application (Δt_{load}=0 sec). Here, the final load torque is applied during the first transient cycle, leading to a more abrupt governor response initiated by the larger speed droop (the latter is due to the greater (engine minus load) torque deficit during the first and the consecutive early transient cycles) resulting in higher fuelings. At the same time, turbocharger lag causes a delay in boost pressure build-up. As a result, higher values of fuel-air equivalence ratios and, thus, in-cycle temperatures are observed, conditions which favor both NO and soot formation. On the contrary, a slower load application causes smoother response of the engine and exhaust emissions, lowering the turbocharger lag effect.

The effect of the load (resistance) type (exponent ‘s’ in equation (20)) on transient NO and soot emissions is illustrated in Figure 11. The stronger the dependence of the load torque on speed (equation (20)), the smaller the speed droop (as shown in Figure 11), since now the load torque $\tau_L(\omega)$ ‘follows’ closely the engine speed response. Consequently, the final equilibrium steady-state conditions are achieved faster. Also, governor response is smoother, leading to lower fueling rates, so that fuel-air equivalence ratios and cylinder temperatures are lower too. The same trend is observed for both NO and soot emissions. On the other hand, a rigid (i.e. speed independent) load is much harder for the engine to cope with, and thus more cycles are needed until the final equilibrium conditions are achieved with increased levels of NO and soot emissions throughout the whole transient event. However, the very high mass moment of inertia of the engine in hand as well as its tight governing, did not allow for the differences to be pronounced.

6.4 Effect of turbocharger parameters

Perhaps the most obvious technique for faster turbocharger, hence engine response, is associated with the former’s rotational moment of inertia. Figure 12 depicts the effect of T/C mass moment of inertia on NO and soot emissions during transient operation after a load increase; turbocharger speed response and fuel-air equivalence ratio development are also given for comparison purposes. Reduction of T/C inertia is one of the simplest strategies in order to improve transient response. This can be seen in Figure 12 by the faster T/C speed development, for the case of reducing its inertia to one fifth of its nominal value (turbocharger frame was kept constant). In that case boost pressure develops faster, and so fuel-air equivalence ratio assumes lower peak values giving accordingly lower NO and soot emissions peaks. However, the final equilibrium values seem to be practically the same with those of the nominal case (for the current engine set-up). On the other hand, a much greater T/C inertia worsens response, in terms of T/C speed development, producing the different results compared to the reduced T/C inertia case confirming the results of previous researchers [1]. All in all, NO emission appears to be mainly affected by the T/C inertia, while soot emissions are only slightly changed.

A very popular means of improving turbocharged diesel engine transient response is the use of variable geometry turbines. During transient operation (either load or speed increase) the main strategy of the VGT is the reduction of the nozzle area by closing

down the vanes so as to increase the back-pressure and enthalpy drop across the turbine, thereby boosting the compressor operating point. By so doing, faster build-up of the engine air-supply is established, minimizing fuel limiting function and improving driveability and emissions. At the same time, the EGR valve is closed to support filling of the cylinders with fresh air. As soon as the air-supply to the engine has been built-up, gradual opening of the VGT vanes follows in order to prevent over-boosting.

Figure 13 expands the previous results for by presenting the effect of the geometric turbine inlet area on transient NO and soot emissions after an increase in load; the corresponding boost pressure and fuel-air equivalence ratio responses are also illustrated in the same figure. A smaller turbine inlet area improves engine response in terms of boost pressure build-up, as documented in Figure 13. Consequently, lower values of fuel-air equivalence ratio are to be expected (fueling is not affected) and so lower peak temperatures in the cylinder. As a result, NO and soot emissions assume lower values. In the case of a larger turbine inlet area, the contrary effect is produced. However, for both cases the effect seems to be rather weak, especially so regarding soot emission.

7. Summary and conclusions

A comprehensive, two-zone, transient, diesel engine thermodynamic model has been applied for the conduction of an extensive parametric study, in order to evaluate the effect of various parameters on NO and soot emissions during transient operation. The parameters concern engine, load and turbocharger characteristics. Comprehensive modeling of in-cylinder processes has been developed, while detailed equations concerning all engine sub-systems represent the peculiarities of transient operation. For the combustion chemistry, a complete chemical equilibrium scheme is used. NO and soot emissions are calculated based on chemical kinetics consideration and formation and oxidation rates respectively. For the current engine-load configuration, which is characterized by high mass moment of inertia and tight governing, the main findings of the study are summarized below:

- A larger exhaust manifold worsens engine response and increases transient emissions, mainly that of NO.

- Advancing EVO timing increases significantly soot emission (up to almost 50% for the cases examined), while a retarded EVO timing leads to improvement. NO emission is increased in both cases.
- The higher the degree of cylinder wall insulation the higher the NO emission. Soot emission is influenced only moderately.
- High viscosity lubricating oils and low oil temperature increase NO and soot emissions.
- The magnitude of the applied load directly affects transient emissions; increased values of NO and soot emissions are noticed for higher load changes.
- The load-time schedule has a strong impact on the development profile and peak values of exhaust emissions, while the final steady-state values are practically unaffected.
- Speed dependent loads are favorable for lower emissions levels throughout the whole transient event.
- A ten times greater T/C mass moment of inertia worsens significantly transient response and exhaust emissions (mainly NO).
- A smaller turbine inlet area improves slightly exhaust emissions, but the effect of the turbine inlet area is generally weak.

Table 1 summarizes the previous results concerning the relative change in peak and cumulative (for all cycles up to equilibrium) values of NO and soot emissions for the cases examined, compared to the nominal case (load change 10-80%, load change duration 1.3 sec, cast iron wall, no insulation, engine running on SAE 30 oil at fully warmed-up conditions, quadratic load type). It is suspected that even greater differences between the cases examined exist, which could not be revealed due to the high mass moment of inertia of the engine in hand. However, similar trends are to be expected. A comprehensive experimental validation of the model's exhaust emissions results is under way by the present research group.

References

[1] Rakopoulos CD, Giakoumis EG. Review of thermodynamic diesel engine simulations under transient operating conditions. SAE Paper no. 2006-01-0884; 2006. Also, SAE Transactions, J Engines 2006;115:467-504.

[2] Watson N, Janota MS. Turbocharging the internal combustion engine, London: McMillan;1982.

[3] Winterbone DE. Transient performance. In: Horlock JH, Winterbone DE, editors. The thermodynamics and gas dynamics of internal combustion engines. Vol. II, Oxford: Clarendon Press; 1986, p.1148-212.

[4] Filipi Z, Wang Y, Assanis D. Effect of variable geometry turbine (VGT) on diesel engine and vehicle system transient response. SAE Paper no. 2001-01-1247; 2001.

[5] Watson N. Eliminating rating effects on turbocharged diesel engine response. SAE Paper no. 840134; 1984.

[6] Rakopoulos CD, Michos CN, Giakoumis EG. Study of the transient behaviour of turbocharged diesel engines including compressor surging using a linearized quasi-steady analysis. SAE Paper no. 2005-01-0225; 2005.

[7] Rakopoulos CD, Giakoumis EG. Availability analysis of a turbocharged diesel engine operating under transient load conditions. Energy 2004;29(8):1085-104.

[8] Rakopoulos CD, Giakoumis EG, Dimaratos AM. Evaluation of various dynamic issues during transient operation of turbocharged diesel engine with special reference to friction development. SAE Paper no. 2007-01-0136; 2007.

[9] Kang H, Farell PV. Experimental investigation of transient emissions (HC and NO_x) in a high speed direct injection (HSDI) diesel engine. SAE Paper no. 2005-01-3883; 2005.

[10] Hagena JR, Filipi ZS, Assanis DN. Transient diesel emissions: analysis of engine operation during a tip-in. SAE Paper no. 2006-01-1151; 2006.

[11] Bazari Z. Diesel exhaust emissions prediction under transient operating conditions. SAE Paper no. 940666; 1994.

[12] Rakopoulos CD, Dimaratos AM, Giakoumis EG, Rakopoulos DC. Exhaust emissions estimation during transient turbocharged diesel engine operation using a two-zone combustion model. Int J Vehicle Design, 2008 (in press).

[13] Chan SH, He Y, Sun JH. Prediction of transient nitric oxide in diesel exhaust. Proc Inst Mech Engrs, J Autom Engng 1999;213(4):327-39.

[14] Cui Y, Deng K, Wu J. A modelling and experimental study of transient NO_x emissions in turbocharged direct injection diesel engines. Proc Inst Mech Engrs, J Autom Engng 2004;218(5):535-41.

[15] Rakopoulos CD, Rakopoulos DC, Kyritsis DC. Development and validation of a comprehensive two-zone model for combustion and emissions formation in a DI diesel engine. Int J Energy Research 2003;27:1221-49.

[16] Rakopoulos CD, Rakopoulos DC, Giakoumis EG, Kyritsis DC. Validation and sensitivity analysis of a two-zone diesel engine model for combustion and emissions prediction. Energy Convers Manage 2004; 45:1471-95.

[17] Heywood JB. Internal combustion engine fundamentals. New York: McGraw Hill;1988.

[18] Benson RS, Whitehouse ND. Internal combustion engines. Oxford: Pergamon Press;1979.

[19] Annand WJD, Ma TH. Instantaneous heat transfer rates to the cylinder head surface of a small compression ignition engine. Proc Inst Mech Engrs 1970-71;185:976-87.

[20] Ferguson CR. Internal combustion engines. New York: Wiley; 1986.

[21] Shahed SM, Chiu WS, Lyn WT. A mathematical model of diesel combustion. In: Combustion in Engines, Institution of Mechanical Engineers, Paper C94/75, 1975. p. 119-28.

[22] Rakopoulos CD, Giakoumis EG, Rakopoulos DC. Study of the short-term cylinder wall temperature oscillations during transient operation of a turbocharged diesel engine with various insulation schemes. Int J Engine Research 2008;9:177-93.

[23] Whitehouse ND, Way RGB. Rate of heat release in diesel engines and its correlation with fuel injection data. Proc Inst Mech Engrs (Part 3J) 1969-70;184:17-27.

[24] Way RJB. Methods for determination of composition and thermodynamic properties of combustion products for internal combustion engine calculations. Proc Inst Mech Engrs 1977;190:687-97.

[25] Lavoie GA, Heywood JB, Keck JC. Experimental and theoretical study of nitric oxide formation in internal combustion engines. Combust Sci Technol 1970;1:313-26.

[26] Hiroyasu H, Kadota T, Arai M. Development and use of a spray combustion modelling to predict diesel engine efficiency and pollutant emissions. Bulletin JSME 1983; 26:569-83.

[27] Lipkea WH, DeJoode AD. Direct injection diesel engine soot modelling: formulation and results. SAE Paper no. 940670; 1994.

Parameter		Peak values		Cumulative values	
		NO	Soot	NO	Soot
Exhaust manifold volume	1/5th	-1.4%	–	-1.1%	–
	10fold	25.1%	5.2%	9.9%	3.0%
EVO timing	30°CA advanced	11.4%	49.0%	44.9%	37.4%
	20°CA retarded	15.9%	-9.6%	7.0%	1.9%
Insulation	4.0 mm SN	7.3%	1.3%	2.6%	–
	1.0 mm PSZ	17.5%	1.8%	10.4%	1.4%
	1.5 mm PSZ	23.4%	3.7%	16.2%	2.6%
Lubricating oil	SAE 30 at 30°C	4.5%	3.4%	–	–
	SAE 20W50 at 40°C	7.8%	15.4%	54.5%	53.4%
Final load	65%	-8.0%	-15.4%	-17.1%	-12.5%
	90%	1.8%	7.5%	47.9%	43.8%
Load change duration	0 sec	11.7%	8.2%	66.4%	59.4%
	3.0 sec	-3.1%	-8.5%	-17.4%	-5.0%
Load type	Rigid, s=0	5.4%	6.6%	95.3%	88.8%
	Linear, s=1	2.6%	3.7%	1.5%	1.8%
T/C mass moment of inertia	1/5th	-11.2%	-2.0%	–	–
	10fold	21.5%	4.5%	7.7%	2.4%
Turbine inlet area	-10%	-3.8%	–	–	–
	+10%	6.7%	1.1%	-1.0%	–

Figures Captions

Fig. 1 Experimental and predicted engine transient response to an increase in engine load.

Fig. 2 Development of various engine and turbocharger variables during the nominal 10-80% load increase transient.

Fig. 3 Development of nitric oxide concentration in the exhaust, maximum values of mean gas temperature and oxygen concentration in the fuel spray during the nominal 10-80% load increase transient.

Fig. 4 Development of soot density in the exhaust, maximum values of mean gas temperature and fuel-air equivalence ratio during the nominal 10-80% load increase transient.

Fig. 5 Effect of exhaust manifold volume on NO concentration and soot density in the exhaust and mean exhaust manifold pressure response.

Fig. 6 Development of NO concentration and soot density in the exhaust, boost pressure and fuel-air equivalence ratio for various exhaust valve opening timings.

Fig. 7 Development of NO concentration and soot density in the exhaust, and mean gas-side cylinder wall temperature for various cylinder wall insulation schemes.

Fig. 8 Effect of lubricating oil type and temperature on NO concentration and soot density in the exhaust, engine speed response and fmep development.

Fig. 9 Effect of load change magnitude on NO concentration and soot density in the exhaust, and the respective cumulative (up to the final equilibrium steady-state cycle) masses exhausted.

Fig. 10 Development of NO concentration and soot density in the exhaust and engine speed and fuel pump rack position responses for various load-time schedules.

Fig. 11 Effect of load type on NO concentration and soot density in the exhaust, fuel-air equivalence ratio development and engine speed response.

Fig. 12 Effect of turbocharger mass moment of inertia on NO concentration and soot density in the exhaust, fuel-air equivalence ratio development and turbocharger speed response.

Fig. 13 Effect of geometric turbine inlet area on NO concentration and soot density in the exhaust, fuel-air equivalence ratio development and boost pressure response.

Table Caption

Table 1 Percentage change of peak and cumulative exhaust emissions values for the cases examined, compared to the nominal case.

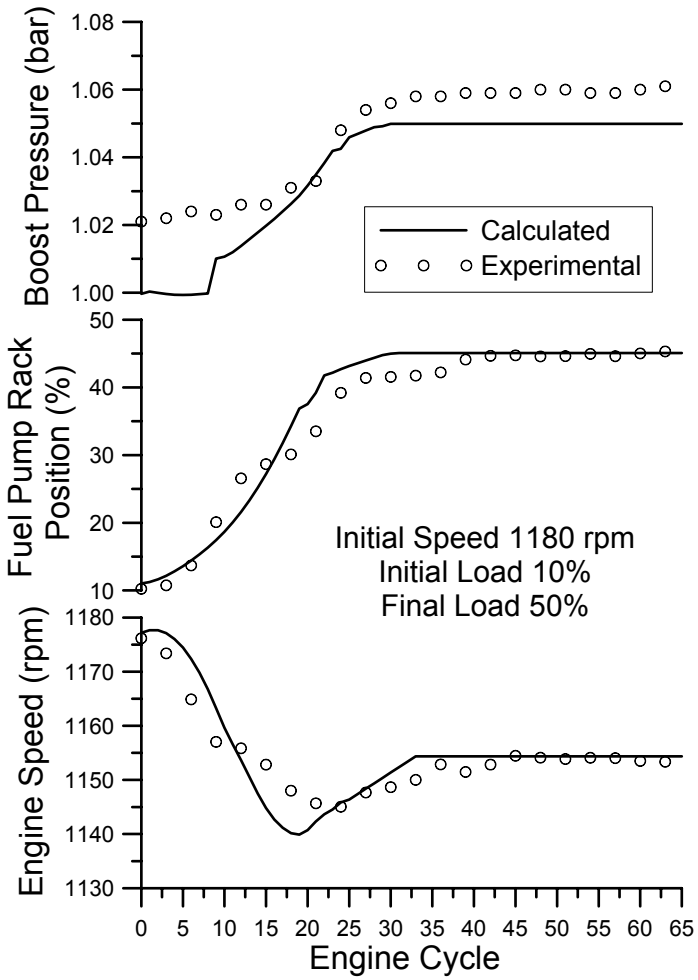
Boost Pressure (bar)
1.08
1.06
1.04
1.02
1.00
Calculated
Experimental
Fuel Pump Rack Position (%)
50
40
30
20
10
Initial Speed 1180 rpm
Initial Load 10%
Final Load 50%
Engine Speed (rpm)
1180
1170
1160
1150
1140
1130
0 5 10 15 20 25 30 35 40 45 50 55 60 65
Engine Cycle

Fig. 1.

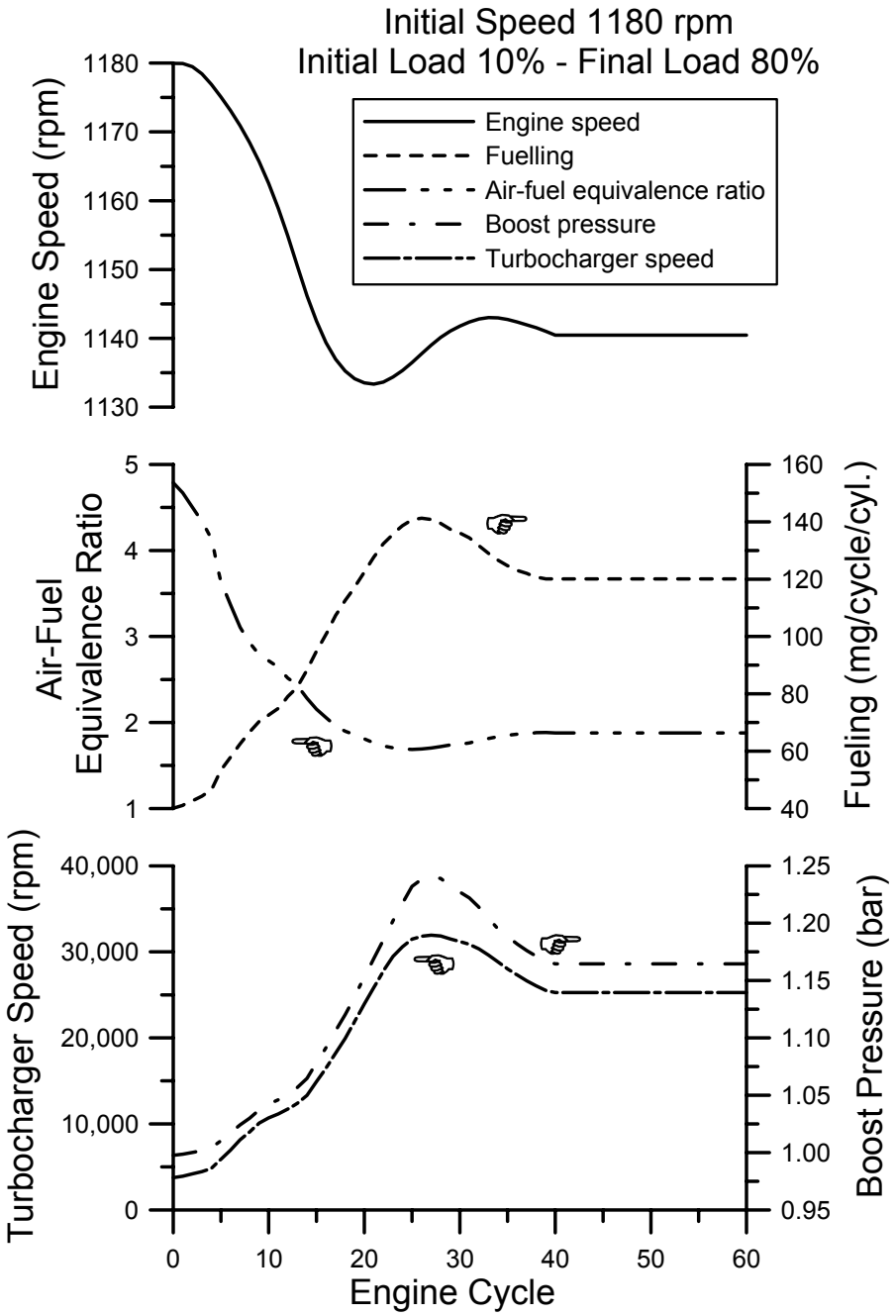
Initial Speed 1180 rpm
Initial Load 10% - Final Load 80%
Engine speed
Fuelling
Air-fuel equivalence ratio
Boost pressure
Turbocharger speed
Engine Speed (rpm)
1180
1170
1160
1150
1140
1130
Air-Fuel Equivalence Ratio
5
4
3
2
1
Fueling (mg/cycle/cyl.)
160
140
120
100
80
60
40
Turbocharger Speed (rpm)
40,000
30,000
20,000
10,000
0
Boost Pressure (bar)
1.25
1.20
1.15
1.10
1.05
1.00
0.95
0
10
20
30
40
50
60
Engine Cycle

Fig. 2.

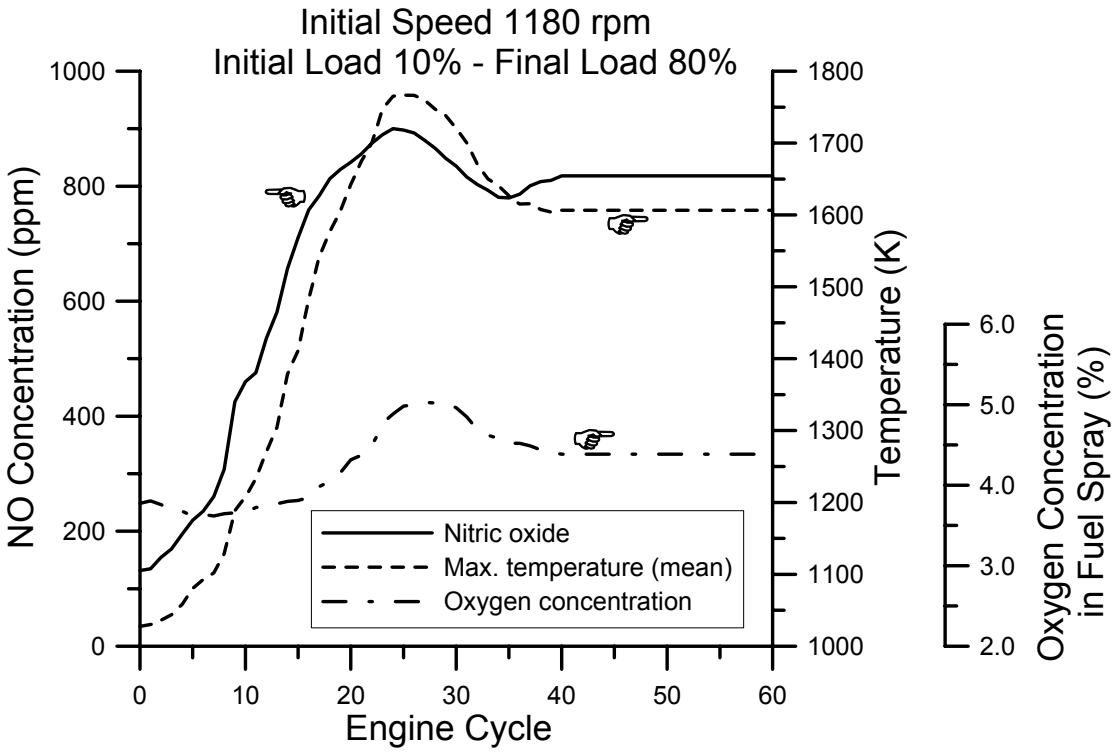
Initial Speed 1180 rpm
Initial Load 10% - Final Load 80%
NO Concentration (ppm)
Temperature (K)
Oxygen Concentration in Fuel Spray (%)
Engine Cycle
Nitric oxide
Max. temperature (mean)
Oxygen concentration
0
200
400
600
800
1000
1000
1100
1200
1300
1400
1500
1600
1700
1800
2.0
3.0
4.0
5.0
6.0
0
10
20
30
40
50
60

Fig. 3.

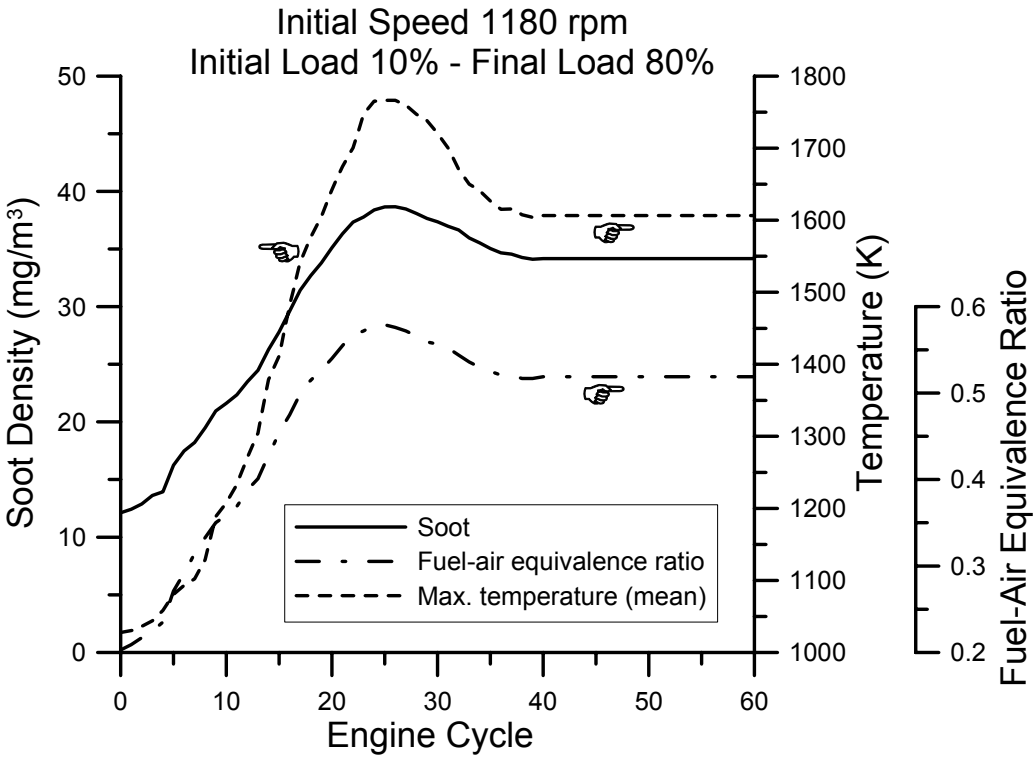
Initial Speed 1180 rpm
Initial Load 10% - Final Load 80%
Soot Density (mg/m³)
Temperature (K)
Fuel-Air Equivalence Ratio
Engine Cycle
Soot
Fuel-air equivalence ratio
Max. temperature (mean)
0
10
20
30
40
50
60
1000
1100
1200
1300
1400
1500
1600
1700
1800
0.2
0.3
0.4
0.5
0.6

Fig. 4.

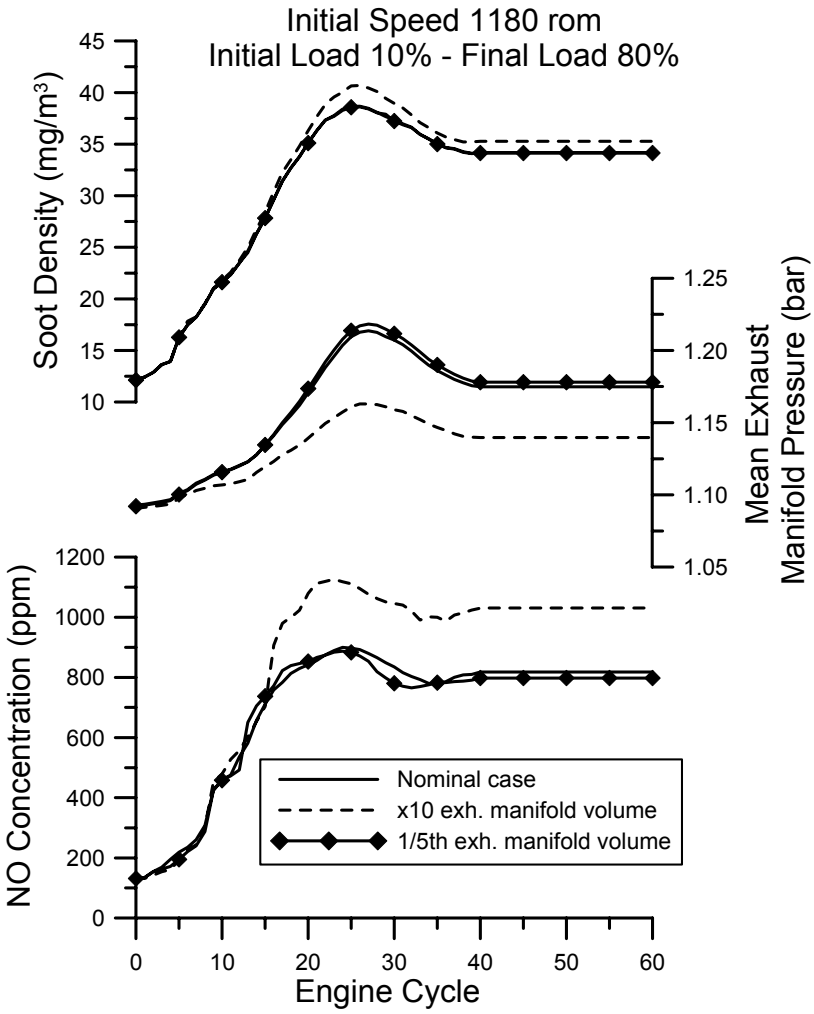
Initial Speed 1180 rom
Initial Load 10% - Final Load 80%
Soot Density (mg/m3)
Mean Exhaust Manifold Pressure (bar)
NO Concentration (ppm)
Engine Cycle
Nominal case
x10 exh. manifold volume
1/5th exh. manifold volume

Fig. 5.

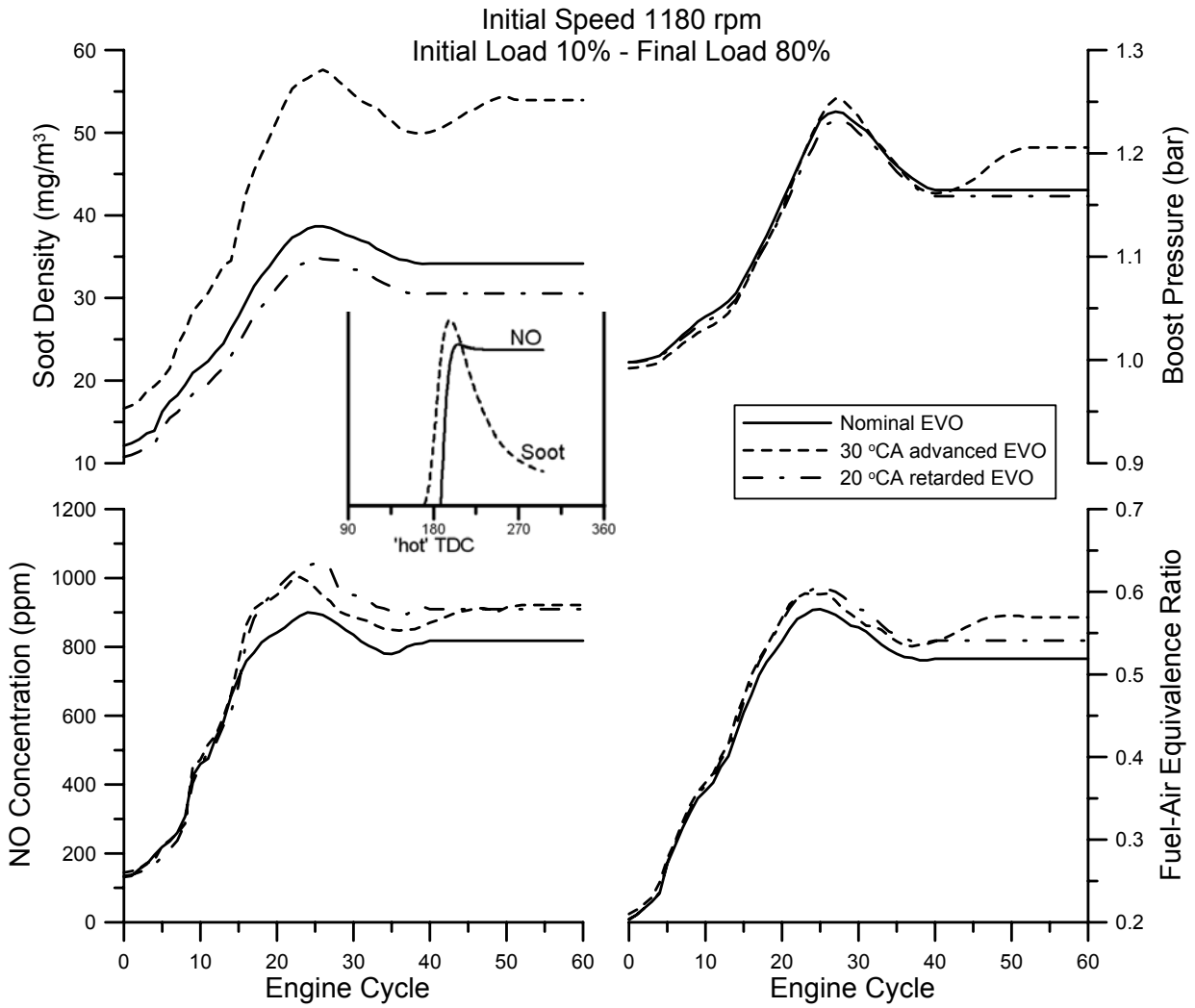
Initial Speed 1180 rpm
Initial Load 10% - Final Load 80%
Soot Density (mg/m³)
Boost Pressure (bar)
NO Concentration (ppm)
Fuel-Air Equivalence Ratio
Engine Cycle
Engine Cycle
NO
Soot
'hot' TDC
Nominal EVO
30 °CA advanced EVO
20 °CA retarded EVO

Fig. 6.

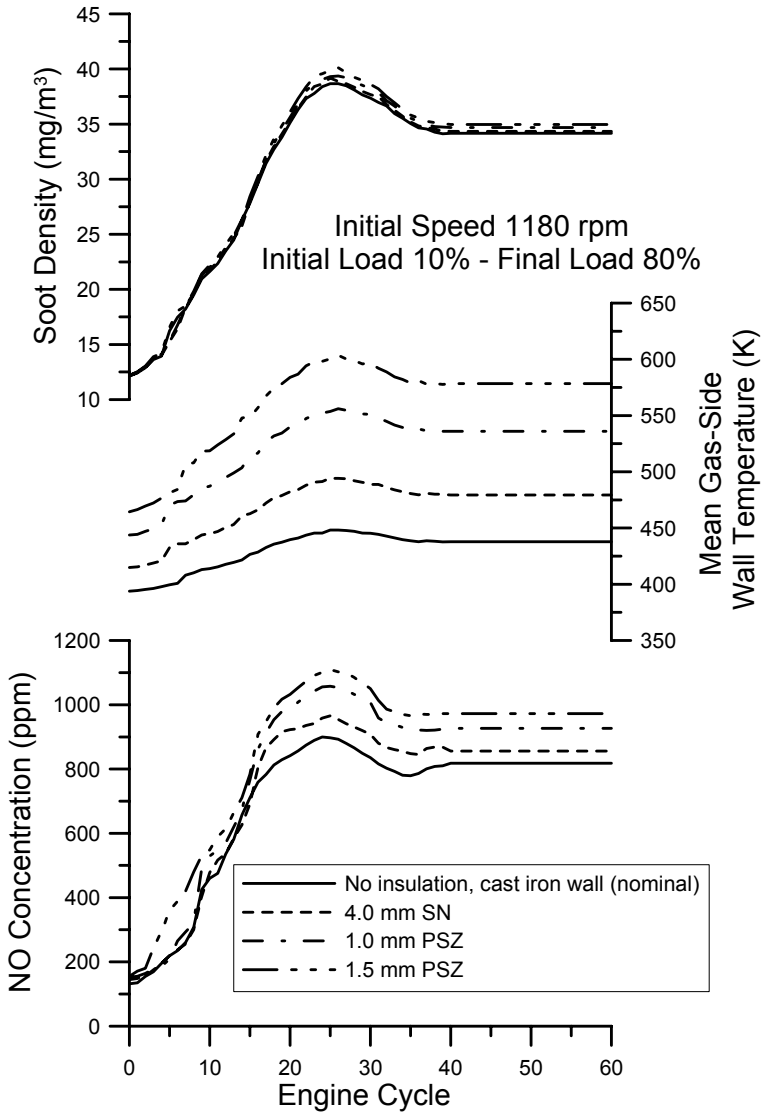
Soot Density (mg/m3)
Initial Speed 1180 rpm
Initial Load 10% - Final Load 80%
Mean Gas-Side Wall Temperature (K)
NO Concentration (ppm)
No insulation, cast iron wall (nominal)
4.0 mm SN
1.0 mm PSZ
1.5 mm PSZ
Engine Cycle

Fig. 7.

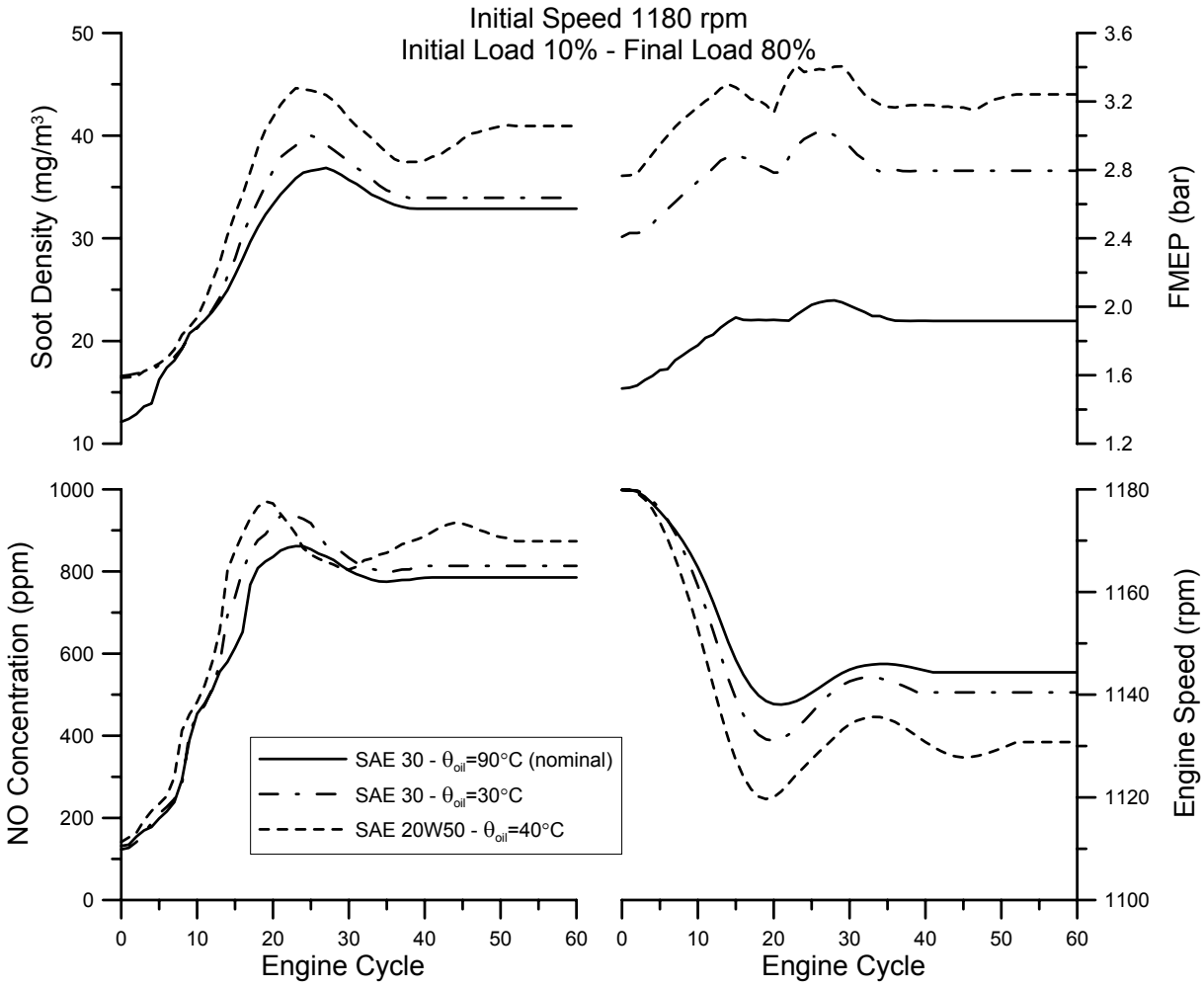
Initial Speed 1180 rpm
Initial Load 10% - Final Load 80%
Soot Density (mg/m³)
FMEP (bar)
NO Concentration (ppm)
Engine Speed (rpm)
Engine Cycle
Engine Cycle
SAE 30 - θoil=90°C (nominal)
SAE 30 - θoil=30°C
SAE 20W50 - θoil=40°C

Fig. 8.

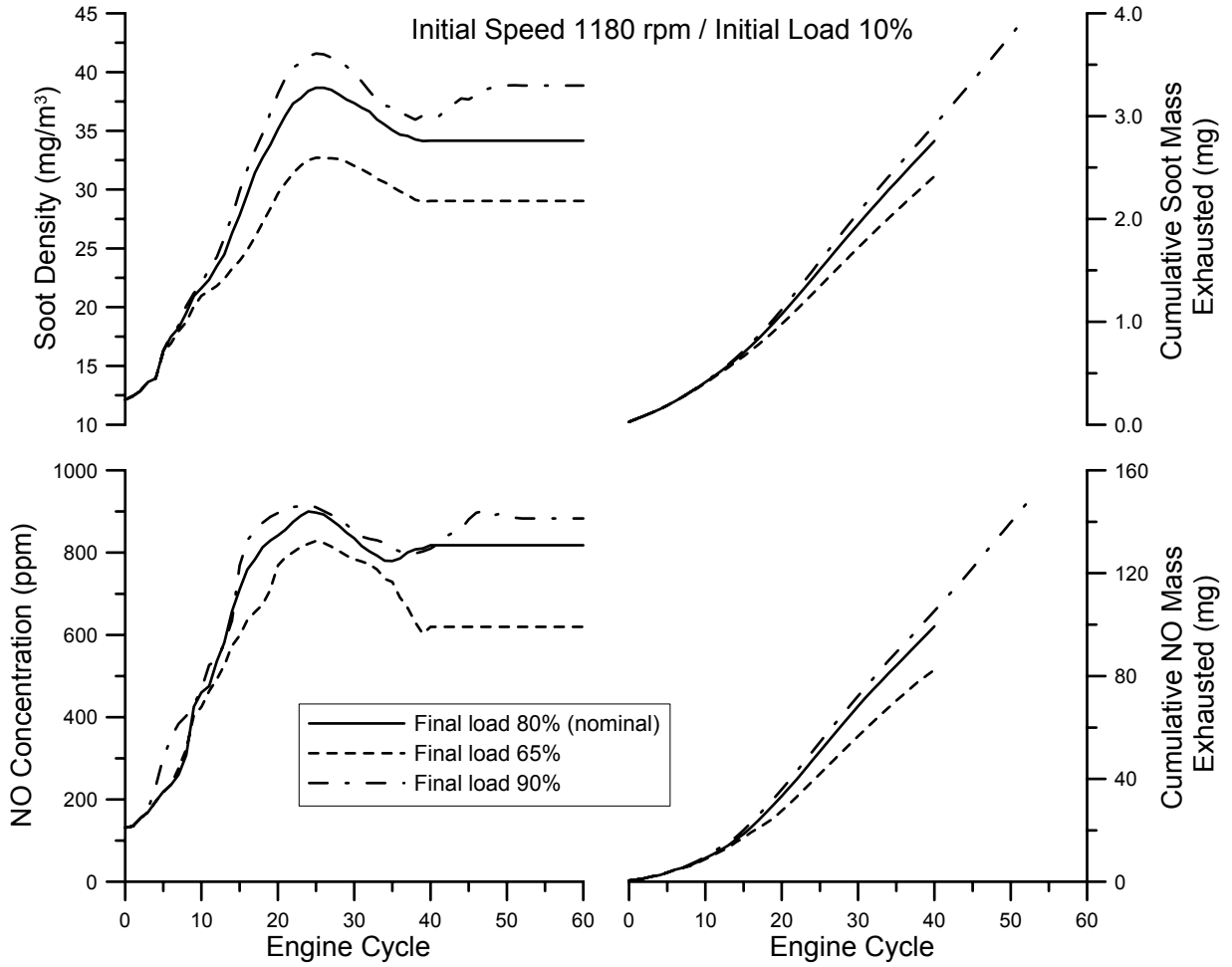
Initial Speed 1180 rpm / Initial Load 10%
Soot Density (mg/m3)
Cumulative Soot Mass Exhausted (mg)
NO Concentration (ppm)
Cumulative NO Mass Exhausted (mg)
Engine Cycle
Engine Cycle
Final load 80% (nominal)
Final load 65%
Final load 90%

Fig. 9.

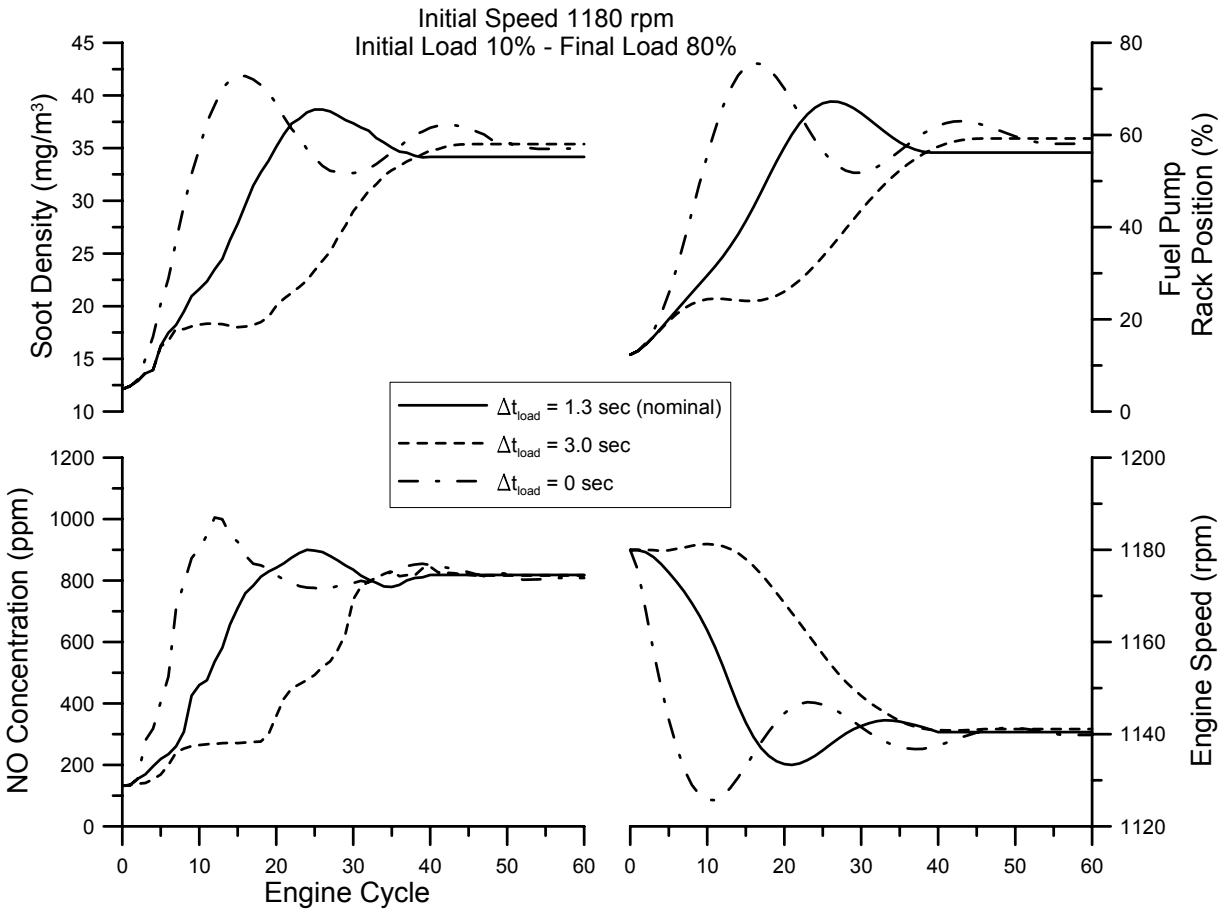
Initial Speed 1180 rpm
Initial Load 10% - Final Load 80%
Soot Density (mg/m³)
Fuel Pump Rack Position (%)
NO Concentration (ppm)
Engine Speed (rpm)
Engine Cycle
Δt_load = 1.3 sec (nominal)
Δt_load = 3.0 sec
Δt_load = 0 sec

Fig. 10.

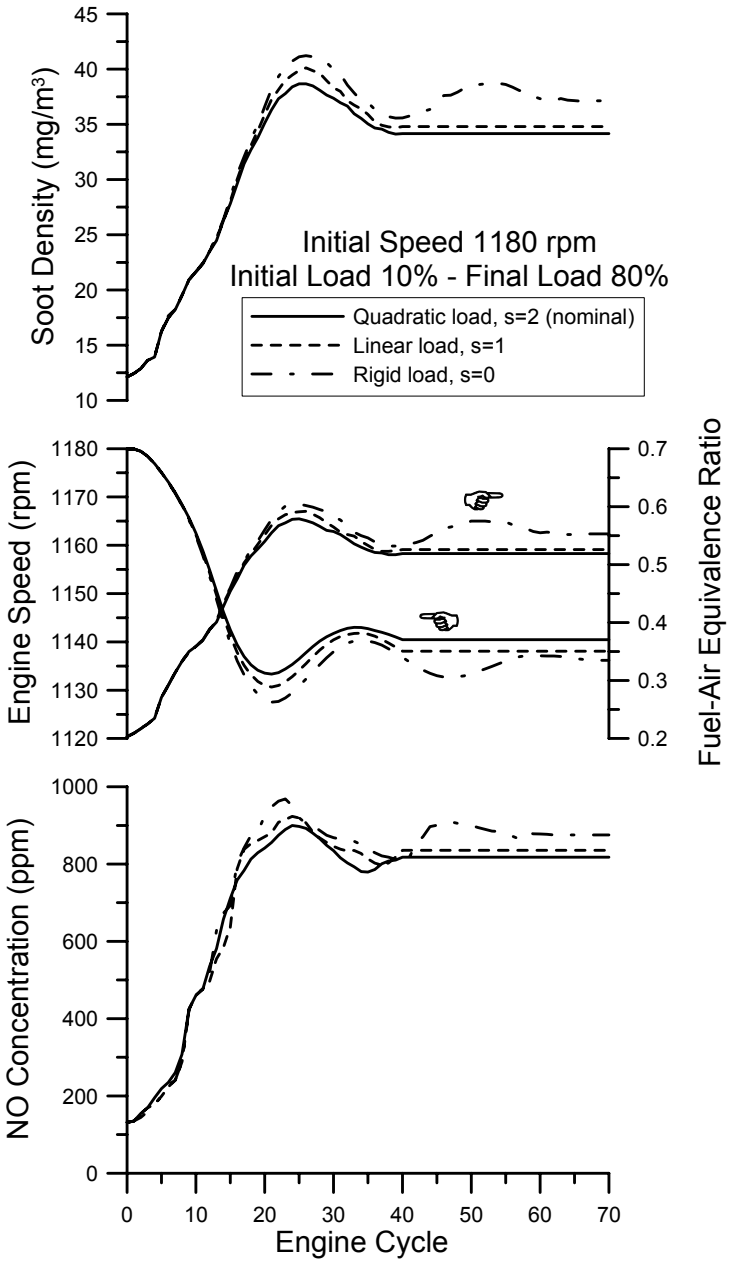
Soot Density (mg/m3)
Initial Speed 1180 rpm
Initial Load 10% - Final Load 80%
Quadratic load, s=2 (nominal)
Linear load, s=1
Rigid load, s=0
Engine Speed (rpm)
Fuel-Air Equivalence Ratio
NO Concentration (ppm)
Engine Cycle

Fig. 11.

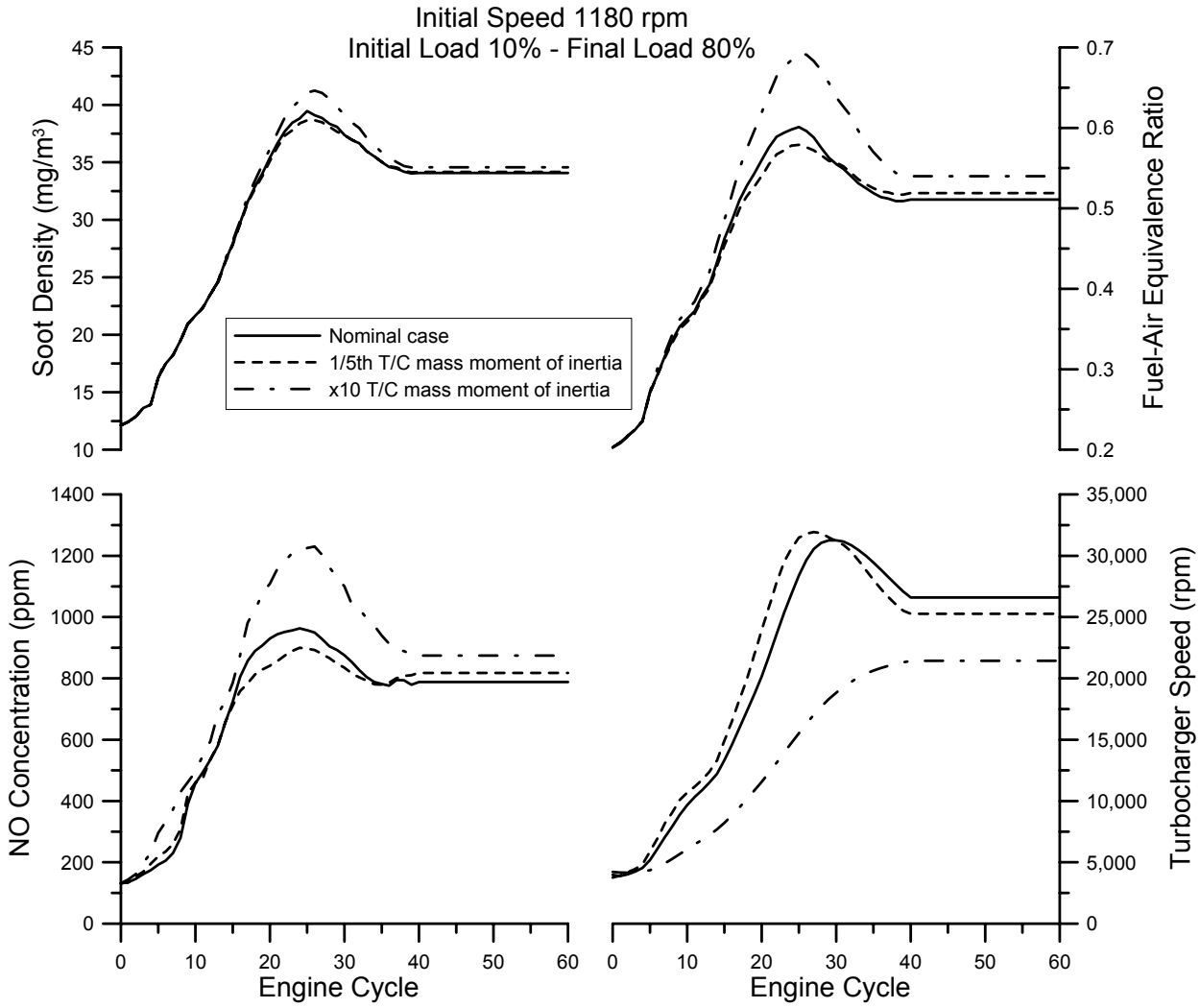
Initial Speed 1180 rpm
Initial Load 10% - Final Load 80%
Soot Density (mg/m3)
Fuel-Air Equivalence Ratio
NO Concentration (ppm)
Turbocharger Speed (rpm)
Engine Cycle
Engine Cycle
Nominal case
1/5th T/C mass moment of inertia
x10 T/C mass moment of inertia

Fig. 12.

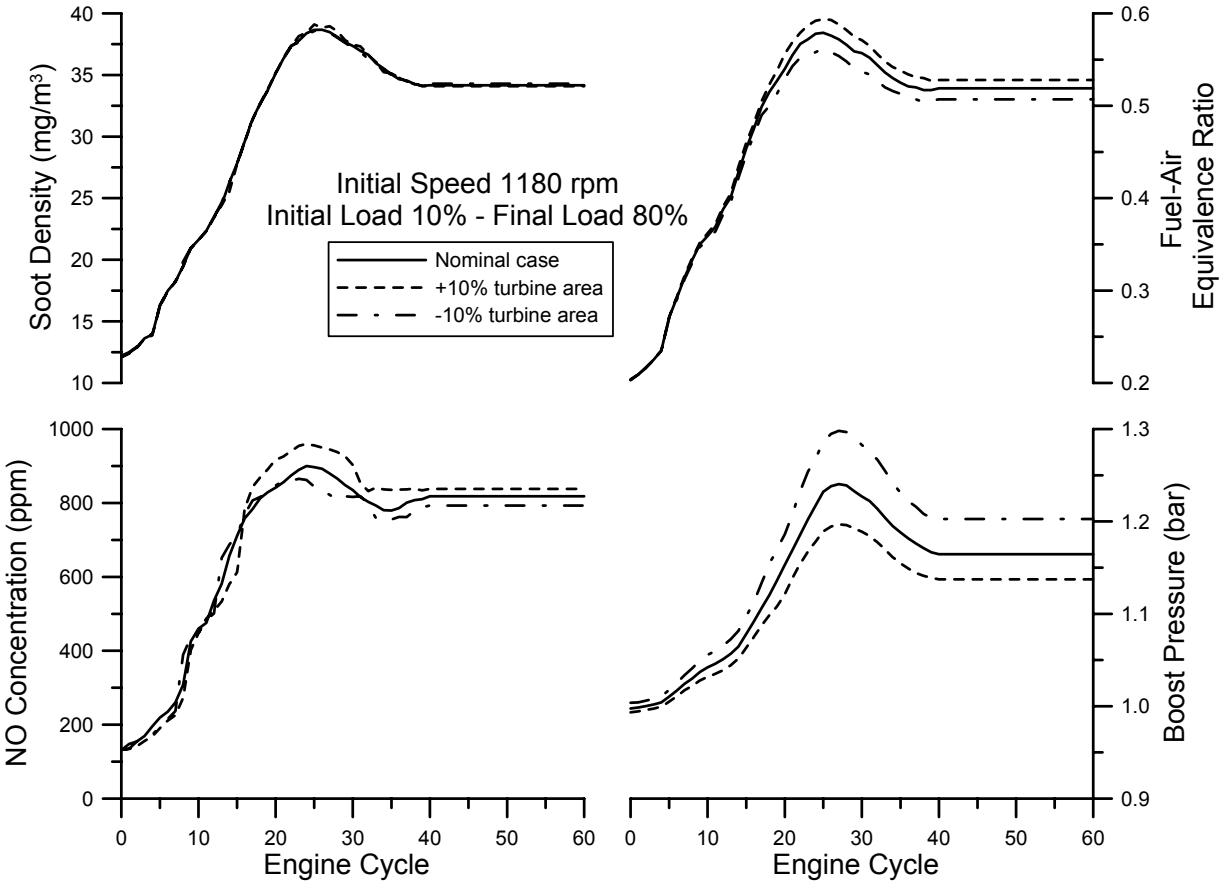
Soot Density (mg/m³)
Initial Speed 1180 rpm
Initial Load 10% - Final Load 80%
Nominal case
+10% turbine area
-10% turbine area
Fuel-Air Equivalence Ratio
NO Concentration (ppm)
Boost Pressure (bar)
Engine Cycle
Engine Cycle

Fig. 13.